IEEE Access
Multidisciplinary | Rapid Review | Open Access Journal

Received 6 October 2023, accepted 16 October 2023, date of publication 23 October 2023, date of current version 31 October 2023.

Digital Object Identifier 10.1109/ACCESS.2023.3326446

RESEARCH ARTICLE

Design of Complex-Order PI/PID Speed Controllers and Its FPAA Realization

MARY ANN GEORGE[1,2], AHMED S. ELWAKIL[3,4,5], (Senior Member, IEEE), ANIS ALLAGUI[2,6,7], AND COSTAS PSYCHALINOS[8], (Senior Member, IEEE)

[1]School of Engineering and IT, Manipal Academy of Higher Education (MAHE), Dubai, United Arab Emirates
[2]Center for Advanced Materials Research, Research Institute of Sciences and Engineering, University of Sharjah, Sharjah, United Arab Emirates
[3]Department of Electrical and Computer Engineering, University of Sharjah, Sharjah, United Arab Emirates
[4]Nanoelectronics Integrated Systems Center (NISC), Nile University, Giza 12677, Egypt
[5]Department of Electrical and Software Engineering, University of Calgary, Alberta, AB T2N 1N4, Canada
[6]Department of Sustainable and Renewable Energy Engineering, University of Sharjah, Sharjah, United Arab Emirates
[7]Department of Mechanical and Materials Engineering, Florida International University, Miami, FL 33174, USA
[8]Electronics Laboratory, Department of Physics, University of Patras, Rio, 26504 Patras, Greece

Corresponding author: Ahmed S. Elwakil (elwakil@ieee.org)

ABSTRACT Complex-order controllers are a generalized version of conventional integer-order controllers and are known to offer greater flexibility, better robustness, and improved system performance. This paper discusses the design of complex-order PI/PID controllers to control the speed of an induction motor drive and an electric vehicle. The speed-tracking performance of the complex-order controllers is compared with fractional-order controllers and conventional integer-order controllers. Implementing complex-order controllers is challenging due to commercial complex-order fractance element unavailability. Hence, it is carried out by approximating the complex-order controller transfer function using an integer-order rational function with a curve-fitting approach, namely the Sanathanan Koener (SK) iterative method. This method is quite simple and can fit the required frequency range compared to the conventional Matsuda and Oustaloup approaches. The approximated controller transfer function can easily be realized by employing the AN231E04 Field Programmable Analog Array (FPAA). Simulation and experimental results highlight that the controller behaviour is in good agreement with the theoretical expectations.

INDEX TERMS Complex-order controllers, speed control, field programmable analog array, fractional-order systems.

LIST OF ABBREVIATIONS

The following abbreviations are used:

ACO	Ant Colony Optimization.
CAB	Configurable Analog Blocks.
CAM	Configurable Analog Modules.
CO[PID]	Complex-order PID.
EV	Electric Vehicle.
FOPDT	First-order Plus Delay Time.
FOPID	Fractional-order PID.
FPAA	Field Programmable Analog Array.
IAE	Integral Absolute Error.
IM	Induction Motor.
ISE	Integral Square Error.
ISCO	Integral Square Controller Output.
ITAE	Integral Time Absolute Error.
ITSE	Integral Time Square Error.
NEDC	New European Drive Cycle.
PFE	Partial Fraction Expansion.
SK	Sanathanan-Koener.
TRAS	Twin-Rotor Aerodynamic System.
VSI	Voltage Source Inverter.

The associate editor coordinating the review of this manuscript and approving it for publication was Ton Duc Do.

I. INTRODUCTION

PID controllers are widely used in industrial applications due to their simplicity, robustness, and various tuning possibilities [1], [2] and are still an active subject of research

interest. The fractional-order PID (FOPID) controller is an extension of the traditional integer-order PID controller with its integral and differential actions having two extra degrees of freedom λ, $\mu \in [0,1]$. This results in better robustness, improved system performance, and design flexibility [3], [4]. The fractional-order controller provides attractive solutions in various control applications; it is well-suited for controlling dynamic systems [5] such as controlling the speed and position in motor drives [4], [6], satellite attitude system [7], robotic manipulators [8], twin-rotor aerodynamic system (TRAS) [9], and electrohydraulic servo system [10].

To further improve the freedom of tuning FOPID controllers, integral and derivative actions of complex-order have been studied by Bingi et al. [11], [12]. Furthermore, Abdulwahhab [13] proposed a complex-order PID controller for a first-order plus time delay (FOPDT) and demonstrated its superiority over conventional controllers to achieve the design specifications more accurately. A power-law FO[PI] controller with reduced active element was suggested in [14], and a power-law FO[PD] controller for robust motion control was proposed in [15]. It was observed that the power law FO[PI]/FO[PD] controller outperformed both conventional PI/PD and FOPI/FOPD controllers.

To further expand the reach of traditional controllers, the main contribution of the paper is the design and study of two power-law complex-order controllers (CO[PI] and CO[PID]) for speed control of induction motor (IM) drive and electric vehicle (EV), respectively. The resulting controller transfer functions are implemented using a Field Programmable Analog Array (FPAA) device. The FPAA gives a cost-effective solution to designers in realizing complex analog circuits [16]. The fractional-order operators/ complex-order operators depend numerically on past values of fractionally derived functions. Hence, the digital realization of complex-order operators requires high computational resources and memory capacity. Moreover realization using FPGA can also lead to performance degradation due to discretization in synthesizing digital controllers [17]. This paper is structured as follows. Section II presents the transfer functions of the complex-order controller models, followed by an analysis of two design applications in Section III. The approximation and realization of the complex-order controllers are presented in Section IV, and controller behavior and performance assessment through simulation and experiments are outlined in Section V.

II. COMPLEX-ORDER CONTROLLER

A. COMPLEX -ORDER OPERATORS

The fractional-order differentiator $D(s)$ and fractional-order integrator $I(s)$ with order $\gamma \in [0, 1]$ are given in the frequency domain by

$$D(s) = s^{\gamma} \tag{1}$$

$$I(s) = \frac{1}{s^{\gamma}} \tag{2}$$

respectively. The complex-order differentiator and complex-order integrator with order $\gamma + j\delta$ ($\gamma \in [0, 1], \delta \in R$) are given respectively by

$$D(s) = s^{\gamma+j\delta} \tag{3}$$

$$I(s) = \frac{1}{s^{\gamma+j\delta}} \tag{4}$$

Writing the complex frequency s in (3)-(4) as $s = j\omega$, we get

$$D(j\omega) = (j\omega)^{\gamma+j\delta} = j^{\gamma}\omega^{\gamma}j^{j\delta}\omega^{j\delta} \tag{5}$$

$$I(j\omega) = \frac{1}{(j\omega)^{\gamma+j\delta}} = \frac{1}{j^{\gamma}\omega^{\gamma}j^{j\delta}\omega^{j\delta}} \tag{6}$$

The terms $j^{j\delta}$ and $\omega^{j\delta}$ in (5) and (6) can be calculated as

$$j^{j\delta} = e^{lnj^{j\delta}} = e^{j\delta(lnj)} = e^{j\delta(\frac{j\pi}{2})} = e^{-\delta\frac{j\pi}{2}} \tag{7}$$

$$\omega^{j\delta} = e^{ln\omega^{j\delta}} = e^{j\delta ln\omega} = \cos(\delta \ln \omega) + j\sin(\delta \ln \omega) \tag{8}$$

By substituting (7) and (8) in (5) and (6), we get,

$$D(j\omega) = j^{\gamma}\omega^{\gamma}e^{-\delta\frac{j\pi}{2}}(\cos(\delta \ln \omega) + j\sin(\delta \ln \omega)) \tag{9}$$

$$I(j\omega) = \frac{1}{j^{\gamma}\omega^{\gamma}e^{-\delta\frac{j\pi}{2}}(\cos(\delta \ln \omega) + j\sin(\delta \ln \omega))} \tag{10}$$

$$= \frac{\cos(\delta \ln \omega) - j\sin(\delta \ln \omega)}{j^{\gamma}\omega^{\gamma}e^{-\delta\frac{j\pi}{2}}} \tag{11}$$

The core issue with the practical realization of complex-order differentiator or integrator is the approximation of complex-order parameters. Oustaloup approximation [18], Matsuda approximation [19], and the Carlson approach [20] are the most widely used frequency-domain methods to determine the approximate integer-order transfer functions for a given fractional-order system. However, these methods are cumbersome and do not necessarily provide the best approximation, given their limitation in the required frequency range. Also, these methods are not suitable for approximating fractional-order differentiators or integrators of complex orders. Following Bingi et al. [12] curve-fitting-based approach for the approximation of the FOPID controller of complex orders, here the functions (9) and (10) are approximated by means of the Sanathanan-Koener (SK) iterative method [21], [22]. The first step in this technique is to determine the frequency response data from (9) for $\omega \in [\omega_l, \omega_h]$.

Next, the integer-order transfer function model $D(s)$ is obtained from using the SK iterative method. Therefore, the approximated $D(s)$ is defined as follows:

$$D(s) = \frac{E(s)}{F(s)} \approx \frac{\sum_{i=0}^{N} e_i s^i}{1 + \sum_{i=0}^{N} f_i s^i} \approx \frac{E\phi(s)}{1 + F\theta(s)} \tag{12}$$

with the coefficients $E = [e_0, e_1, \ldots, e_N]^T$, $F = [f_0, f_1, \ldots, f_N]^T$ (T for transpose), and the monomial functions $\phi(s) = \left[1, s, \ldots s^N\right]$, $\theta(s) = \left[s, s^2, \ldots s^N\right]$. Finally,

the coefficient of E and F are determined considering the following Levy's objective function with SK iteration:

$$arg \min_{E,F} \sum_{p=l}^{h} \left| \frac{E(j\omega_p)}{F^{T-1}(j\omega_p)} - \frac{F^T(j\omega_p)}{F^{T-1}(j\omega_p)} H(j\omega_p) \right|^2 \quad (13)$$

where T is the iteration step. By solving (13), unbiased fitting is achieved when $F^{T-1}(j\omega_p)$ approaches $F^T(j\omega_p)$. Here, the curve-fitting-based technique uses the built-in functions of MATLAB software *frd* and *fitfrd* for extracting and processing the frequency response data for an order N.

B. COMPLEX-ORDER PID CONTROLLER

The transfer function of a FOPID is given by

$$C(s) = K_p + \frac{K_i}{s^\lambda} + K_d s^\mu \quad (14)$$

where K_p, K_i and K_d are controller gains and λ, μ ($0 \leq \lambda, \mu \leq 1$) orders of the integrator and differentiator stages, respectively. A complex FOPID controller [13] is then obtained by allowing the order of the integrator and differentiator stages to be complex numbers rather than real numbers. Its transfer function is

$$C(s) = K_p + \frac{K_i}{s^{\lambda+j\phi}} + K_d s^{\mu+j\theta} \quad (15)$$

where $0 \leq \lambda, \mu \leq 1, \phi, \theta \in \mathbb{R}$.

Similarly, the transfer function of the corresponding power-law FO[PID] controller is given by

$$C(s) = \left(K_p + \frac{K_i}{s} + K_d s \right)^\gamma \quad (16)$$

where $0 \leq \gamma \leq 1$. Therefore, the transfer function of the proposed complex-order [PID] (CO[PID]) controller is defined as

$$C(s) = \left(K_p + \frac{K_i}{s} + K_d s \right)^{\gamma+j\delta} \quad (17)$$

where $0 \leq \gamma \leq 1, \delta \in \mathbb{R}$. By substituting $K_i = 0$ or $K_d = 0$, the respective transfer function of complex-order [PI] (CO[PI]) and complex-order [PD] (CO[PD]) controllers are obtained.

III. APPLICATION EXAMPLES

A. DESIGN EXAMPLE 1-INDUCTION MOTOR SPEED CONTROL

The fractional-order voltage source inverter (VSI) fed induction motor (IM) model is described by [23]:

$$G(s) = \frac{279.18s^{1.87} + 2224s^{0.9} + 33750}{s^{2.97} + 22.21s^{1.89} + 138.7s^{0.94} + 438.6} \quad (18)$$

The CO[PI] controller $C(s)$ is designed to control the speed of the IM plant model in (18). The magnitude and phase of (18) are:

$$|G(j\omega)| = \frac{\sqrt{(P^2 + Q^2)}}{\sqrt{(R^2 + S^2)}} \quad (19)$$

$$\angle G(j\omega) = \tan^{-1}\left(\frac{Q}{P}\right) - \tan^{-1}\left(\frac{S}{R}\right) \quad (20)$$

respectively, where

$$P = 279.18\omega^{1.87}\cos\left(\frac{1.87\pi}{2}\right) + 2224\omega^{0.9}\cos\left(\frac{0.9\pi}{2}\right) + 33750;$$

$$Q = 279.18\omega^{1.87}\sin\left(\frac{1.87\pi}{2}\right) + 2224\omega^{0.9}\sin\left(\frac{0.9\pi}{2}\right);$$

$$R = \omega^{2.97}\cos\left(\frac{2.97\pi}{2}\right) + 22.21\omega^{1.89}\cos\left(\frac{1.89\pi}{2}\right) + 138.7\omega^{0.94}\cos\left(\frac{0.94\pi}{2}\right) + 438.6;$$

$$S = \omega^{2.97}\sin\left(\frac{2.97\pi}{2}\right) + 22.21\omega^{1.89}\sin\left(\frac{1.89\pi}{2}\right) + 138.7\omega^{0.94}\sin\left(\frac{0.94\pi}{2}\right);$$

Furthermore, we have:

$$\frac{d}{d\omega}(\angle G(j\omega)) = \frac{1}{\left(\frac{Q}{P}\right)^2 + 1}\frac{D_Q P - Q D_P}{P^2} + \frac{1}{\left(\frac{S}{R}\right)^2 + 1}\frac{D_S R - S D_R}{R^2} \quad (21)$$

where

$$D_P = 521.606\omega^{0.87}\cos\left(\frac{1.87\pi}{2}\right) + 2090.56\omega^{-0.1}\cos\left(\frac{0.9\pi}{2}\right);$$

$$D_Q = 521.606\omega^{0.87}\sin\left(\frac{1.87\pi}{2}\right) + 2090.56\omega^{-0.1}\sin\left(\frac{0.9\pi}{2}\right);$$

$$D_R = 2.97\omega^{1.97}\cos\left(\frac{2.97\pi}{2}\right) + 41.977\omega^{0.89}\cos\left(\frac{1.89\pi}{2}\right) + 130.38\omega^{-0.06}\cos\left(\frac{0.94\pi}{2}\right);$$

$$D_S = 2.97\omega^{1.97}\sin\left(\frac{2.97\pi}{2}\right) + 41.977\omega^{0.89}\sin\left(\frac{1.89\pi}{2}\right) + 130.38\omega^{-0.06}\sin\left(\frac{0.94\pi}{2}\right);$$

As for the design constraints we wish to have for a robust complex controller, first, the open loop gain $H(s)$ of the plant model is equal to 0 dB at the gain crossover frequency (ω_{cg}), i.e.

$$|H(j\omega_{gc})| = |G(j\omega_{gc})|\,|C(j\omega_{gc})| = 1 \quad (22)$$

Second, the expression for phase margin $\phi_m$is given by

$$\angle G(j\omega_{gc})\angle C(j\omega_{gc}) = -\pi + \phi_m \quad (23)$$

Combining (22) and (23), we get

$$G(j\omega_{gc})C(j\omega_{gc}) = 1\angle(\phi_m - \pi) \tag{24}$$

and

$$C(j\omega_{gc}) = \frac{e^{j(\phi_m - \pi - \angle G(j\omega_{gc})}}{\left|G(j\omega_{gc})\right|} \tag{25}$$

where $e^{j(\phi_m-\pi-\angle G(j\omega_{gc})} = \cos\left(\phi_m - \pi - \angle G(j\omega_{gc})\right) + j\sin\left(\phi_m - \pi - \angle G(j\omega_{gc})\right)$. Third, the constraint to improve the controller's robustness during gain variation is given by:

$$\frac{d}{d\omega}\angle G(j\omega_{gc}) + \frac{d}{d\omega}\angle C(j\omega_{gc}) = 0 \tag{26}$$

Now the transfer function model for the controller (CO[PI]) is given by

$$C(s) = (K_p + \frac{K_i}{s})^{(\gamma+j\delta)} \tag{27}$$

By using Taylor's series expansion and neglecting higher order terms (28), the function can be approximated by

$$C_1(s) = (K_i)^{\gamma+j\delta}\left[\frac{1 + (\gamma + j\delta)\frac{K_p}{K_i}s}{s^{(\gamma+j\delta)}}\right] \tag{28}$$

The expressions for magnitude and phase of the CO[PI] controller $C_1(j\omega)$ are given by

$$|C_1(j\omega)| = \sqrt{R^2 + I^2}; \tag{29}$$

$$\angle C_1(j\omega) = \tan^{-1}\left(\frac{I}{R}\right) \tag{30}$$

where

$$\begin{aligned}
R &= \frac{K_i^{\gamma} e^{\frac{\delta\pi}{2}}}{\omega^{\gamma}}[A\cos(\delta\ln K_i) - B\sin(\delta\ln K_i)];\\
I &= \frac{K_i^{\gamma} e^{\frac{\delta\pi}{2}}}{\omega^{\gamma}}[B\cos(\delta\ln K_i) + A\sin(\delta\ln K_i)];\\
A &= \cos(\delta\ln\omega)[\cos(\frac{\gamma\pi}{2}) + \gamma\frac{K_p}{K_i}\omega\sin(\frac{\gamma\pi}{2})\\
&\quad + \delta\frac{K_p}{K_i}\omega\cos(\frac{\gamma\pi}{2})] + \sin(\delta\ln\omega)[-\sin(\frac{\gamma\pi}{2})\\
&\quad + \gamma\frac{K_p}{K_i}\omega\cos(\frac{\gamma\pi}{2}) + \delta\frac{K_p}{K_i}\omega\sin(\frac{\gamma\pi}{2})];\\
B &= \cos(\delta\ln\omega)[-\sin(\frac{\gamma\pi}{2}) + \gamma\frac{K_p}{K_i}\omega\cos(\frac{\gamma\pi}{2})\\
&\quad + \delta\frac{K_p}{K_i}\omega\sin(\frac{\gamma\pi}{2})] - \sin(\delta\ln\omega)[\cos(\frac{\gamma\pi}{2})\\
&\quad + \gamma\frac{K_p}{K_i}\omega\sin(\frac{\gamma\pi}{2}) + \delta\frac{K_p}{K_i}\omega\cos(\frac{\gamma\pi}{2})];
\end{aligned}$$

The differentiation of $\angle C_1(j\omega)$ is

$$\frac{d}{d\omega}(\angle C_1(j\omega)) = \frac{1}{\left(\frac{I}{R}\right)^2 + 1}\frac{D_I R - I D_R}{R^2} \tag{31}$$

where

$$\begin{aligned}
D_I &= K_i^{\gamma} e^{\frac{\delta\pi}{2}}[\omega^{-\gamma} D_B\cos(\delta\ln K_i)\\
&\quad - \gamma\omega^{-\gamma-1}B\cos(\delta\ln K_i) + \omega^{-\gamma} D_A\sin(\delta\ln K_i)\\
&\quad - \gamma\omega^{-\gamma-1}A\sin(\delta\ln K_i)];\\
D_R &= K_i^{\gamma} e^{\frac{\delta\pi}{2}}[\omega^{-\gamma} D_A\cos(\delta\ln K_i)\\
&\quad - \gamma\omega^{-\gamma-1}A\cos(\delta\ln K_i) - \omega^{-\gamma} D_B\sin(\delta\ln K_i)\\
&\quad + \gamma\omega^{-\gamma-1}B\sin(\delta\ln K_i)];\\
D_A &= -\frac{\delta}{\omega}\sin(\delta\ln\omega)\cos(\frac{\gamma\pi}{2})\\
&\quad + \gamma\frac{K_p}{K_i}\sin(\frac{\gamma\pi}{2})\cos(\delta\ln\omega)\\
&\quad - \delta\gamma\frac{K_p}{K_i}\sin(\frac{\gamma\pi}{2})\sin(\delta\ln\omega)\\
&\quad + \delta\frac{K_p}{K_i}\cos(\frac{\gamma\pi}{2})\cos(\delta\ln\omega)\\
&\quad - \delta^2\frac{K_p}{K_i}\cos(\frac{\gamma\pi}{2})\sin(\delta\ln\omega)\\
&\quad - \frac{\delta}{\omega}\sin(\frac{\gamma\pi}{2})\cos(\delta\ln\omega)\\
&\quad + \gamma\frac{K_p}{K_i}\cos(\frac{\gamma\pi}{2})\sin(\delta\ln\omega)\\
&\quad + \delta\gamma\frac{K_p}{K_i}\cos(\frac{\gamma\pi}{2})\cos(\delta\ln\omega)\\
&\quad + \delta\frac{K_p}{K_i}\sin(\frac{\gamma\pi}{2})\sin(\delta\ln\omega)\\
&\quad + \delta^2\frac{K_p}{K_i}\sin(\frac{\gamma\pi}{2})\cos(\delta\ln\omega);\\
D_B &= -\frac{\delta}{\omega}\sin(\frac{\gamma\pi}{2})\sin(\delta\ln\omega)\\
&\quad + \gamma\frac{K_p}{K_i}\cos(\frac{\gamma\pi}{2})\cos(\delta\ln\omega)\\
&\quad - \delta\gamma\frac{K_p}{K_i}\cos(\frac{\gamma\pi}{2})\sin(\delta\ln\omega)\\
&\quad + \delta\frac{K_p}{K_i}\sin(\frac{\gamma\pi}{2})\cos(\delta\ln\omega)\\
&\quad - \delta^2\frac{K_p}{K_i}\sin(\frac{\gamma\pi}{2})\sin(\delta\ln\omega)\\
&\quad - \frac{\delta}{\omega}\cos(\frac{\gamma\pi}{2})\cos(\delta\ln\omega)\\
&\quad - \gamma\frac{K_p}{K_i}\sin(\frac{\gamma\pi}{2})\sin(\delta\ln\omega)\\
&\quad - \delta\gamma\frac{K_p}{K_i}\cos(\frac{\gamma\pi}{2})\cos(\delta\ln\omega)\\
&\quad - \delta\frac{K_p}{K_i}\cos(\frac{\gamma\pi}{2})\sin(\delta\ln\omega)\\
&\quad - \delta^2\frac{K_p}{K_i}\cos(\frac{\gamma\pi}{2})\cos(\delta\ln\omega);
\end{aligned}$$

$$R = \frac{\cos\left(\phi_m - \pi - \angle G(j\omega_{gc})\right)}{|G(j\omega)|} \tag{32}$$

$$I = \frac{\sin\left(\phi_m - \pi - \angle G(j\omega_{gc})\right)}{|G(j\omega)|} \tag{33}$$

The controller parameters of the CO[PI] controller for the VSI-fed IM plant are obtained by solving (32), (33), and (26). Table 1 presents the controller gains of the CO[PI] controller

TABLE 1. Speed Controllers for the IM plant in (18) at $\omega_{cg} = 8$ rad/s and $\phi_m = 30°$ stability boundaries.

Controllers	Controller Transfer Function
PI	$0.0176 + \frac{0.2181}{s}$
FOPI	$0.0257 + \frac{0.1451}{s^{0.865}}$
FO[PI]	$\left[0.017 + \frac{0.1633}{s}\right]^{0.9386}$
CO[PI]	$\left[0.02 + \frac{0.13}{s}\right]^{0.799+0.1i}$

and previously reported controllers (PI, FOPI, FO[PI]). The approximated integer-order transfer functions of the controllers are obtained using curve-fitting approximation (a third-order approximation in the frequency range $\omega = [-0.01, 0.01]$ rad/s is considered). The approximated transfer function for FO[PI] and CO[PI] controllers are given by:

$$C_{FO[PI]}(s) = \frac{0.0224s^3 + 0.2013s^2 + 0.09531s + 0.003124}{s^3 + 0.5888s^2 + 0.02295s + 1.231 \times 10^{-05}} \quad (34)$$

and

$$C_{CO[PI]}(s) = \frac{0.02262s^3 + 0.4843s^2 + 1.158s + 0.06749}{s^3 + 5.896s^2 + 0.6808s + 0.004079} \quad (35)$$

respectively.

B. DESIGN EXAMPLE 2: ELECTRIC VEHICLE (EV) SPEED CONTROL

The EV system dynamics include both vehicle and motor dynamics. The linearized model of EV obtained using system identification by George et al. [24] is described as

$$G_{EV}(s) = \frac{0.01292s^3 + 0.005944s^2 + 0.0004034s + 1.836 \times 10^{-05}}{s^5 + 0.2985s^4 + 0.1139s^3 + 0.01532s^2 + 0.001381s + 4.641 \times 10^{-05}} \quad (36)$$

The CO[PID] controller $C_2(s)$ is designed using the Ant Colony Optimization (ACO) algorithm to control the speed of the EV system. The ACO technique can determine the optimal solution rapidly when more pheromones are released [24], [25]. The pseudocode for ACO is given in Fig. 1.

The upper and lower bounds of controller parameters are chosen as: $K_p = (0, 60)$, $K_i = (0, 60)$, $K_d = (0, 60)$, $\lambda = (0, 1)$, $\mu = (0, 1)$, $\gamma = (0, 1)$, $\delta = (-1, 1)$. The objective function for optimization is selected such that both the error-index and the control signal are minimized and are given by:

$$J = ITSE + ITAE + IAE + ISE + ISCO \quad (37)$$

$$J = \int_0^\infty te^2(t)dt + \int_0^\infty t\,|e(t)|\,dt + \int_0^\infty |e(t)|\,dt + \int_0^\infty e^2(t)dt + \int_0^\infty u^2(t)dt \quad (38)$$

ACO Algorithm
1. ***while*** not terminated
  2. ***for each*** ant in a colony, find a solution
    2.1 set all nodes as unvisited
    2.2 ***while*** number of unvisited nodes > 0 ***do***
      2.3 computes ant's probabilities to visit nodes
      2.4 select a node according to the probabilities
  3. ***if*** decided, apply the local optimization process to the best solution found in a current generation
  4. save the best solution if found
  5. evaporate pheromone trails
  6. update pheromone trail according to the selected solution in a current generation
7. ***return*** the best solution

FIGURE 1. Pseudocode of ACO.

TABLE 2. Speed controllers for EV plant using ACO.

Controllers	Controller Transfer Function
PID	$30 + \frac{2.1}{s} + 50s$
FOPID	$29 + \frac{3.4}{s^{0.9}} + 50s^{0.91}$
FO[PID]	$\left(3.17 + \frac{3.4}{s} + 50s\right)^{0.9}$
CO[PID]	$\left(2.09 + \frac{3.15}{s} + 50s\right)^{0.9-0.01i}$

where ITSE denotes the integral time square error, ITAE the integral time absolute error, IAE the integral absolute error, ISE the integral square error, ISCO the integral square controller output, $e(t)$ the error signal, and $u(t)$ is the control signal. The controller parameters of the CO[PID] controller and other conventional controllers for EV speed control obtained using ACO are presented in Table 2. The third-order approximation in the range $\omega = [-0.01, 0.01]$ rad/s is used for approximating the transfer function of the FO[PID] and CO[PID] controllers as given below:

$$C_{FO[PID]}(s) = \frac{1.745 \times 10^4 s^3 + 2.7 \times 10^5 s^2 + 4.638 \times 10^4 s + 1.766 \times 10^4}{s^3 + 797.1s^2 + 8603s + 16.59} \quad (39)$$

$$C_{CO[PID]}(s) = \frac{9170s^3 + 1.36 \times 10^5 s^2 + 2.33 \times 10^4 s + 7816}{s^3 + 417.8s^2 + 4136s + 3.878} \quad (40)$$

IV. SIMULATIONS AND EXPERIMENTAL RESULTS

The CO[PI] and CO[PID] controllers for IM drive and EV speed control are realized and simulated in MATLAB-Simulink. The open-loop magnitude and phase responses of VSI-fed IM drive using PI, FOPI, FO[PI], and CO[PI] controllers are illustrated in Fig. 2 (a). It is observed that the CO[PI] controller has a higher stability margin at $\omega_{cg} = 8$ rad/s than other controllers. Fig. 2 (b) shows the closed loop speed response of VSI-fed IM with the designed

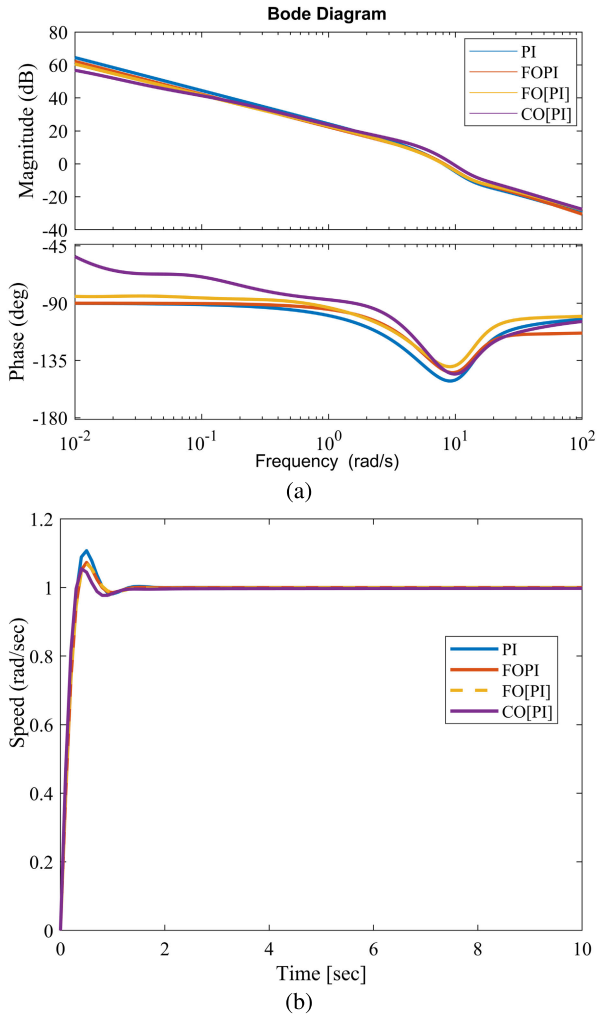

FIGURE 2. (a) Open-loop gain and phase, (b) closed loop speed response of IM drive using PI, FOPI, FO[PI] and CO[PI] controllers.

TABLE 3. Time domain performance of PI, FOPI, FO[PI] and CO[PI] controllers.

Controllers	t_r(s)	t_s(s)	$\%O_s$
PI	0.2403	0.7477	10.7%
FOPI	0.2337	0.7356	7.31%
FO[PI]	0.2330	0.7226	7.05%
CO[PI]	**0.2247**	**0.7186**	**5.74%**

controllers. It is observed the CO[PI] has less settling time (t_s), rise time (t_r), and overshoot ($\%O_s$) compared to other controllers in its speed response. The time domain performance of the proposed CO[PI] controller and other conventional controllers are given in Table 3.

The experimental evaluation of the proposed controllers was performed by employing the Anadigm AN231E04 FPAA development board and the Anadigm Designer 2 EDA software. The FPAA device has a 2 × 2 matrix of fully configurable analog blocks (CABs), which offer design programmability and versatility. The AN231E04 device has seven configurable input and output structures. The detailed architecture of the AN231E04 device and its features are

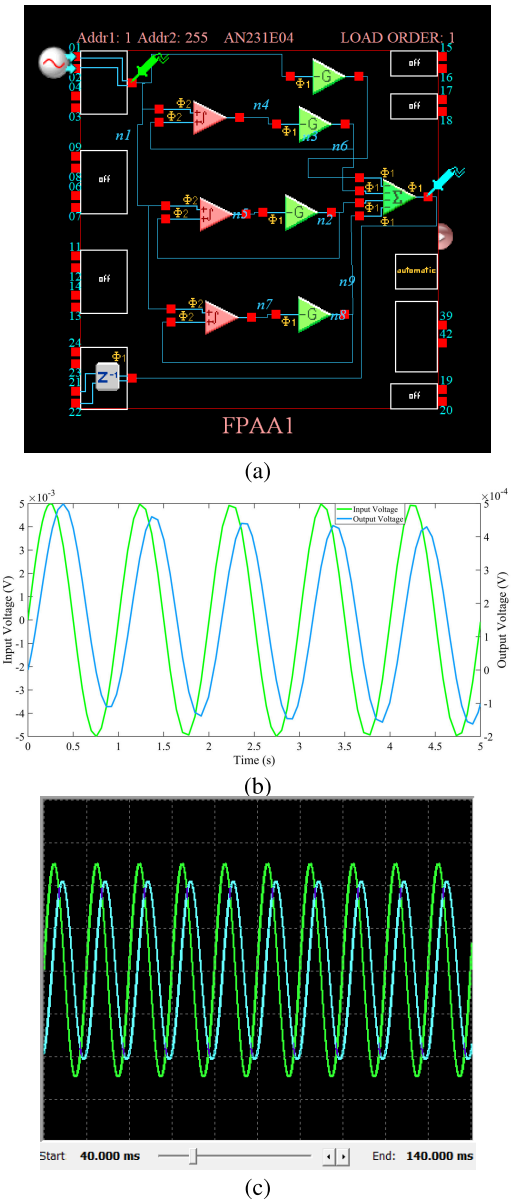

FIGURE 3. (a) FPAA-based realization, (b) simulated results, and (c) experimental results:input (green) and output (blue) waveforms of the approximated CO[PI] controller of order 3, using a sinusoidal signal of peak amplitude 5 mV and frequency of 100 Hz.

given in [26]. First, one can see that the approximated integer-order transfer functions of the CO[PI] and CO[PID] controllers shown in (35) and (40), respectively, have the following general form:

$$H_{approx}(s) = \frac{A_3 s^3 + A_2 s^2 + A_1 s + A_0}{s^3 + B_2 s^2 + B_1 s + B_0} \tag{41}$$

Eq. (41) can be implemented by applying the partial fraction expansion (PFE) technique:

$$H_{PFE} = K_0 + \frac{K_1.\omega_{01}}{s + \omega_{01}} + \frac{K_2.\omega_{02}}{s + \omega_{02}} + \frac{K_3.\omega_{03}}{s + \omega_{03}} \tag{42}$$

It is observed that (42) is a sum of integer-order low-pass filters and a gain factor, where $K_0 = A_3, K_i = \frac{r_i}{|p_i|}$ and

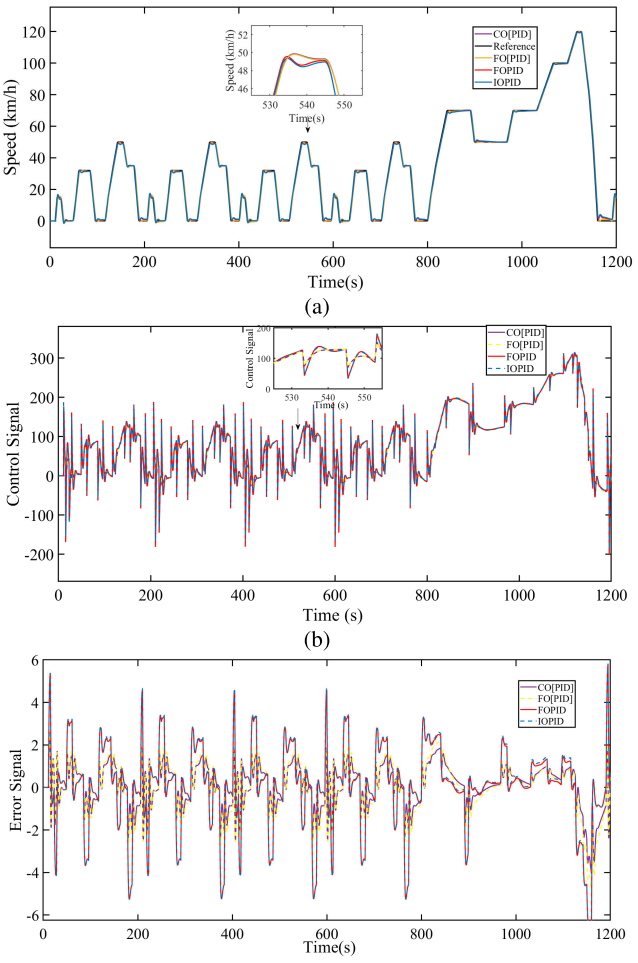

FIGURE 4. (a) Performance of the proposed controllers to track the NEDC cycle, (b) control signals, and (c) error signals.

$\omega_{0i} = |p_i|, i = 1, 2, 3$. The p_i and r_i denotes the poles and residues of (41). Table 4 summarizes the scaling factors (K_i) and time constants ($\tau_i = \frac{1}{\omega_{0i}}$) for CO[PI] and CO[PID] controllers. By substituting K_i and τ_i in (42) the PFE-based approximated transfer function of the controller is obtained. It is then implemented in the Anadigm Designer 2 EDA software using the *SumIntegrator*, *SumDiff*, and *GainHold* configurable analog modules (CAMs). The FPAA board has four AN231E04 chips, and each chip has eight CAMS. As the implementation uses a 3rd-order approximation (Eq. (41)), a single AN231E04 chip is utilized. For an order greater than 3, two or more chips were required. The clock frequency of the chip was chosen as f_{clk}= 800 kHz. The time-domain performance of the controller is verified using a sinusoidal signal of 100 Hz and a peak amplitude of 5 mV. Fig. 3 (a) shows the FPAA-based realization of the CO[PI] controller in the Anadigm design. Fig. 3 (b) shows the simulated result for the 3rd-order approximated CO[PI] controller. Fig. 3 (c) shows the experimental results (the input (green) and output (blue) waveform) for the approximated CO[PI] controller.

EV speed control using CO[PID], FO[PID], FOPID, and IOPID controller is shown in Fig. 4 (a). The New European

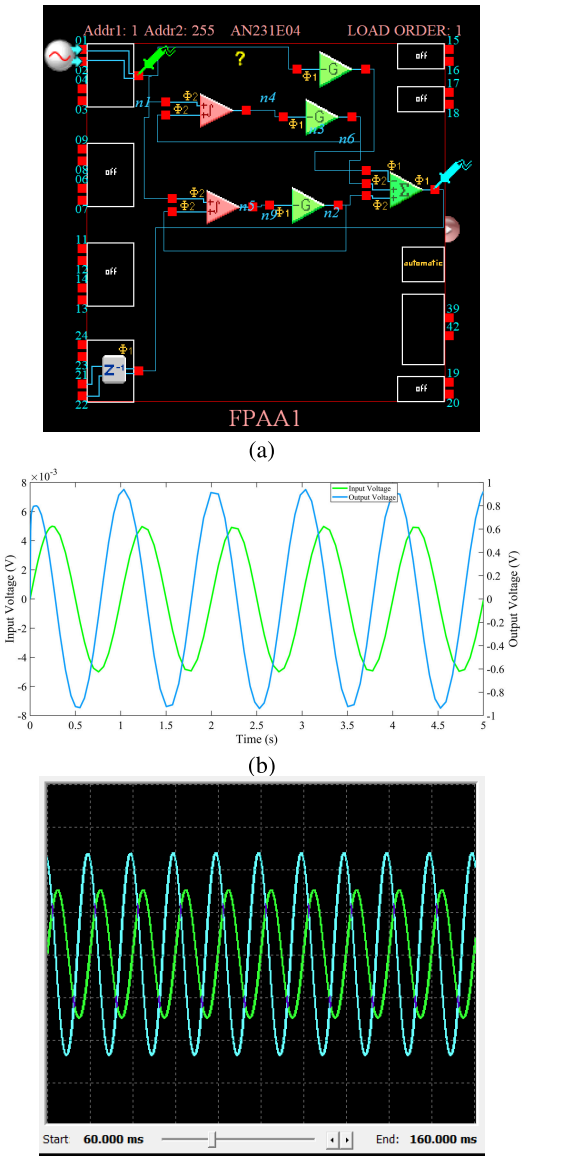

FIGURE 5. (a) FPAA-based realization, (b) simulated results, and (c) experimental results:input (green) and output (blue) waveforms of the approximated CO[PID] controller of order 3, using a sinusoidal signal of peak amplitude 5 mV and frequency of 100 Hz.

TABLE 4. Scaling factors and time constants for realizing CO[PI] and CO[PID] controllers described in [35] and [40], respectively using PFE.

Parameters	CO[PI]	CO[PID]
K_0	0.0226	9170
K_1	0.0274	8829
K_2	0.8375	98.25
K_3	15.761	0
$\tau_1(ms)$	0.1730	0.00245
$\tau_2(ms)$	8.976	0.09825
$\tau_3(ms)$	158.730	0.00670

Drive Cycle (NEDC) test is widely used to test EV speed tracking in India and Europe. Fig. 4 (a) shows that the CO[PID] controller has superior speed tracking performance

TABLE 5. Comparison of simulated and experimental results for CO[PI] and CO[PID] controller using sinusoidal signal of different amplitude.

CO[PI] controller				
Input voltage (pk-pk)	Simulated output voltage (pk-pk)	Experiment output voltage (pk-pk)	Simulated phase shift (Deg)	Experiment phase shift (Deg)
3 mV	0.26 mV	0.25 mV	23.5°	25.3°
5 mV	0.42 mV	0.41 mV	23.5°	25.3°
7 mV	0.613 mV	0.58 mV	23.5°	25.3°
9 mV	0.79 mV	0.74 mV	23.5°	25.3°
CO[PID] controller				
2mV	0.37 V	0.36 V	-37.8°	-39.1°
3 mV	0.55 V	0.54 V	-37.8°	-39.1°
4 mV	0.74 V	0.73 V	-37.8°	-39.1°
5 mV	0.93 V	0.92 V	-37.8°	-39.1°

than other controllers. Fig. 4 (b) and Fig. 4 (c) illustrate the control signals and tracking error of the proposed controllers. It is observed that the CO[PI] controller provides minimum controller effort and tracking error compared to the other controllers.

Finally, Fig. 5 (a) shows the FPAA-based realization of the CO[PID] controllers in the Anadigm design. Fig. 5 (b) shows the simulated results for the 3rd-order approximated CO[PID] controller. Fig. 5 (c) shows experimental results (the input (green) and output (blue) waveform) for the approximated CO[PID] controller. Table 5 shows the simulated and experimental results of CO[PI] and CO[PID] controllers for sinusoidal signals of different amplitudes. It is clearly observed that experimental results closely follow the simulated response.

V. CONCLUSION

The complex-order PI/PID controllers were designed for IM drive using frequency domain specifications and for EV speed control using the ACO algorithm. The complex-order controller performed better than the fractional-order and integer-older counterparts. The approximation of complex-order controller transfer function via a curve fitting approach facilitated an efficient and compact realization. The approximation order was selected equal to three to attain an accurate level of approximation. The approximated transfer function could be easily implemented and experimentally verified using the FPAA platform, exploiting its numerous advantages in performing signal processing operations like integration, differentiation, scaling, and summation. The design procedure is versatile and could be used in a variety of applications, including biological and biomedical systems, for approximating complex-order transfer functions.

REFERENCES

[1] F. Padula and A. Visioli, "Optimal tuning rules for proportional-integral-derivative and fractional-order proportional-integral-derivative controllers for integral and unstable processes," *IET Control Theory Appl.*, vol. 6, no. 6, pp. 776–786, Apr. 2012.

[2] K. H. Ang, G. Chong, and Y. Li, "PID control system analysis, design, and technology," *IEEE Trans. Control Syst. Technol.*, vol. 13, no. 4, pp. 559–576, Jul. 2005.

[3] V. Badri and M. S. Tavazoei, "Some analytical results on tuning fractional-order [proportional-integral] controllers for fractional-order systems," *IEEE Trans. Control Syst. Technol.*, vol. 24, no. 3, pp. 1059–1066, May 2016.

[4] A. Khurram, H. Rehman, S. Mukhopadhyay, and D. Ali, "Comparative analysis of integer-order and fractional-order proportional integral speed controllers for induction motor drive systems," *J. Power. Electron.*, vol. 18, no. 3, pp. 723–735, 2018.

[5] A. Tepljakov, E. A. Gonzalez, E. Petlenkov, J. Belikov, C. A. Monje, and I. Petráš, "Incorporation of fractional-order dynamics into an existing PI/PID DC motor control loop," *ISA Trans.*, vol. 60, pp. 262–273, Jan. 2016.

[6] W. Yu, Y. Luo, Y. Chen, and Y. Pi, "Frequency domain modelling and control of fractional-order system for permanent magnet synchronous motor velocity servo system," *IET Control Theory Appl.*, vol. 10, no. 2, pp. 136–143, Jan. 2016.

[7] W. Xinsheng and Z. Huaqiang, "Fractional order controller for satellite attitude control system with PWPF modulator," in *Proc. 34th Chin. Control Conf. (CCC)*, Jul. 2015, pp. 5758–5763.

[8] R. Sharma, P. Gaur, and A. P. Mittal, "Performance analysis of two-degree of freedom fractional order PID controllers for robotic manipulator with payload," *ISA Trans.*, vol. 58, pp. 279–291, Sep. 2015.

[9] S. Ijaz, M. T. Hamayun, L. Yan, and M. F. Mumtaz, "Fractional order modeling and control of twin rotor aero dynamical system using Nelder Mead optimization," *J. Electr. Eng. Technol.*, vol. 11, no. 6, pp. 1863–1871, Nov. 2016.

[10] S. Ijaz, M. A. Choudhry, A. Ali, and U. Javaid, "Application of fractional order control technique to an electro-hydraulic position servomechanism," *J. Eng. Technol.*, vol. 34, no. 3, pp. 35–44, Aug. 2015.

[11] K. Bingi, A. P. Singh, and B. R. Prusty, "Curve fitting-based approximation of fractional differentiator with complex orders," in *Proc. 3rd Int. Conf. Energy, Power Environ., Towards Clean Energy Technol.*, Mar. 2021, pp. 1–6.

[12] K. Bingi, R. R. Kulkarni, and R. Mantri, "Design and analysis of complex fractional-order PID controllers," in *Proc. IEEE Madras Sect. Conf. (MASCON)*, Aug. 2021, pp. 1–6.

[13] O. W. Abdulwahhab, "Design of a complex fractional order PID controller for a first order plus time delay system," *ISA Trans.*, vol. 99, pp. 154–158, Apr. 2020.

[14] S. Kapoulea, C. Psychalinos, and A. S. Elwakil, "Reduced active element power-law proportional-integral controller designs," in *Proc. 3rd Novel Intell. Lead. Emerg. Sci. Conf. (NILES)*, Oct. 2021, pp. 51–54.

[15] Y. Luo and Y. Chen, "Fractional-order [proportional derivative] controller for robust motion control: Tuning procedure and validation," in *Proc. Amer. Control Conf.*, Jun. 2009, pp. 1412–1417.

[16] A. A. Dastjerdi, B. M. Vinagre, Y. Chen, and S. H. HosseinNia, "Linear fractional order controllers; a survey in the frequency domain," *Annu. Rev. Control*, vol. 47, pp. 51–70, Apr. 2019.

[17] K. Angkeaw, W. Pongyart, and P. Prommee, "Design and implementation of FPAA based LQR controller for magnetic levitation control system," in *Proc. 42nd Int. Conf. Telecommun. Signal Process. (TSP)*, Jul. 2019, pp. 411–414.

[18] A. Oustaloup, F. Levron, B. Mathieu, and F. M. Nanot, "Frequency-band complex noninteger differentiator: Characterization and synthesis," *IEEE Trans. Circuits Syst. I, Fundam. Theory Appl.*, vol. 47, no. 1, pp. 25–39, Jan. 2000.

[19] D. Valério, J. J. Trujillo, M. Rivero, J. A. T. Machado, and D. Baleanu, "Fractional calculus: A survey of useful formulas," *Eur. Phys. J. Special Topics*, vol. 222, no. 8, pp. 1827–1846, Sep. 2013.

[20] A. Tepljakov, E. Petlenkov, and J. Belikov, "Application of Newton's method to analog and digital realization of fractional-order controllers," *Int. J. Microelectron. Comput. Sci.*, vol. 3, no. 2, pp. 45–52, 2012.

[21] J. Nako, C. Psychalinos, and A. S. Elwakil, "Complex-order controller design examples and their implementation," *Int. J. Circuit Theory Appl.*, pp. 1–10, Jul. 2023, doi: 10.1002/cta.3751.

[22] K. Bingi, R. Ibrahim, M. N. Karsiti, S. M. Hassam, and V. R. Harindran, "Frequency response based curve fitting approximation of fractional-order PID controllers," *Int. J. Appl. Math. Comput. Sci.*, vol. 29, no. 2, pp. 311–326, Jun. 2019.

[23] S. Adigintla and M. V. Aware, "Robust fractional order speed controllers for induction motor under parameter variations and low speed operating regions," *IEEE Trans. Circuits Syst. II, Exp. Briefs*, vol. 70, no. 3, pp. 1119–1123, Mar. 2023.
[24] M. A. George, D. V. Kamat, and C. P. Kurian, "Electronically tunable ACO based fuzzy FOPID controller for effective speed control of electric vehicle," *IEEE Access*, vol. 9, pp. 73392–73412, 2021.
[25] A. Mughees and S. A. Mohsin, "Design and control of magnetic levitation system by optimizing fractional order PID controller using ant colony optimization algorithm," *IEEE Access*, vol. 8, pp. 116704–116723, 2020.
[26] C. Muñiz-Montero, L. A. Sánchez-Gaspariano, C. Sánchez-López, V. R. González-Díaz, and E. Tlelo-Cuautle, "On the electronic realizations of fractional-order phase-lead-lag compensators with OpAmps and FPAAs," in *Fractional Order Control and Synchronization of Chaotic Systems*. Berlin, Germany: Springer, 2017, pp. 131–164.

MARY ANN GEORGE received the bachelor's degree in electronics and communication engineering and the master's degree in digital electronics and advanced communication from the Manipal Institute of Technology (MIT), Manipal Academy of Higher Education (MAHE), Manipal, Karnataka, India, in 2013 and 2016, respectively, and the Ph.D. degree in electronics and communication engineering from MAHE, in 2022. She is currently a Research Assistant with the University of Sharjah, United Arab Emirates. She is also an Adjunct Faculty Member of MAHE, Dubai, United Arab Emirates. Her research interests include fractional-order controllers, fractional-order systems, and analog circuits. She is a Life Member of the Indian Society of Systems for Science and Engineering (ISSE).

AHMED S. ELWAKIL (Senior Member, IEEE) was born in Cairo, Egypt. He received the B.Sc. and M.Sc. degrees in electronics and communications from Cairo University, Egypt, and the Ph.D. degree in electrical and electronic engineering from the National University of Ireland, University College Dublin. He also held visiting positions with Istanbul Technical University, Turkey; Queens University, Belfast, U.K.; the Technical University of Denmark, Lyngby, Denmark; and the King Abdullah University of Science and Technology, Saudi Arabia. He is currently a Full Professor with the University of Sharjah, United Arab Emirates; also with the University of Calgary, AB, Canada; and also with the Nanoelectronics Integrated Systems Center (NISC), Nile University, Cairo. He has authored or coauthored more than 350 publications. His research interests include circuit theory, nonlinear dynamics, chaos theory, and fractional-order circuits and systems with diverse applications ranging from the modeling of oscillatory networks and nonlinear behavior in electronic circuits and plasma physics to modeling of energy storage devices, bio-materials, and biological tissues. He has been a member of the IEEE Technical Committee on Nonlinear Circuits and Systems, since 2000. He was a recipient of the Egyptian Government First Class Medal for achievements in engineering sciences, in 2015, and the UAE President Award (Khalifa Award), in 2020. He is also an International Observer in the European Cooperation in Science and Technology (COST) action on fractional-order system analysis synthesis and their importance for future design (CA15225) and an Expert with the United Nations Development Program (UNDP). He was on the editorial board of the IEEE Journal on Emerging and Selected Topics in Circuits and Systems and an Associate Editor of IEEE Transactions on Circuits and Systems—I: Regular Papers. He currently serves as the Editor-in-Chief for the *International Journal of Circuit Theory and Applications* (Wiley) and an Associate Editor for the *International Journal of Electronics and Telecommunications* (AEUE, Elsevier).

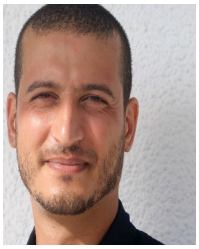

ANIS ALLAGUI received the M.Eng. degree in engineering mechanics from Ecole Polytechnique of Nantes, France, in 2007, and the Ph.D. degree in mechanical engineering from Concordia University, Montreal, Canada, in 2011. He continued as a FQRNT Postdoctoral Fellow for two years with the University of Ottawa, Canada. He has been with the University of Sharjah, United Arab Emirates, since 2013, where he is currently an Associate Professor. He has been also a Courtesy Associate Professor with Florida International University, Miami, USA, since 2020. His research interests include the design and modeling of electrochemical energy storage in supercapacitors and batteries using fractional-order calculus and physics-based models.

COSTAS PSYCHALINOS (Senior Member, IEEE) received the B.Sc. and Ph.D. degrees in physics and electronics from the University of Patras, Greece, in 1986 and 1991, respectively. From 1993 to 1995, he was a Postdoctoral Researcher with the VLSI Design Laboratory, University of Patras, where he was an Adjunct Lecturer with the Department of Computer Engineering and Informatics, from 1996 to 2000. From 2000 to 2004, he was an Assistant Professor with the Electronics Laboratory, Department of Physics, Aristotle University of Thessaloniki, Greece. Since 2004, he has been a Faculty Member of the Electronics Laboratory, Department of Physics, University of Patras. Currently, he is a full professor. His research interests include the development of CMOS analog integrated circuits, including fractional-order circuits and systems, continuous and discrete-time analog filters, amplifiers, and low voltage/low power building blocks for analog signal processing. He is a member of the Nonlinear Circuits and Systems Technical Committee of the IEEE CAS Society. He serves as the Editor-in-Chief for the Circuit and Signal Processing Section for the *Electronics* journal (MDPI). He serves as an Area Editor for the *International Journal of Electronics and Communications* (AEUE) and an Editor for the *International Journal of Circuit Theory and Applications*. He is an Associate Editor of the *Circuits, Systems, and Signal Processing* and the *Journal of Advanced Research*. He is a member of the Editorial Board of the *Microelectronics Journal*, *Analog Integrated Circuits and Signal Processing*, *IETE Journal of Education*, *Fractal and Fractional*, and *Journal of Low Power Electronics and Applications*.